Arch. Metall. Mater. **69** (2024), 2, 507-513

DOI: https://doi.org/10.24425/amm.2024.149777

SHI JIN[1], GUANYU CHEN[1], XIN HUANG[2], GUOFU OU[2*]

STUDY ON CORROSION BEHAVIOR OF SOUR WATER STRIPPER IN AMMONIUM CHLORIDE BY ELECTROCHEMICAL TECHNIQUES

The corrosion features of 20# carbon steel, the base material of sour water stripper, in NH_4Cl solution were examined in this research. The anatomical samples of the corroded parts were characterized by an X-ray diffractometer and other analytical tools. It was found to be a localized perforation caused by pitting, and the corrosion product was $FeCl_2$. 20# steel was subjected to electrochemical testing using Tafel polarization and Electrochemical impedance spectroscopy. The studies showed that the 20# steel's cathodic depolarization reaction rate speeds as density rises, and that the concentration polarization gets more marked as temperature rises. The corrosion rate of 20# steel is the fastest when temperature hits its highest point of 80°C, measuring 4.7142 mm/a. When density rose from 5 to 20%, corrosion rate grew from 1.6378 to 7.2430 mm/a.

Keywords: Stripper; NH_4Cl corrosion; Electrochemical testing; carbon steel

1. Introduction

Crude oil has tended to get heavier and lesser quality over the past few years, with higher levels of corrosives including sulfur, nitrogen, and chlorine. The operating circumstances of the equipment are drastically altered by changes in the characteristics of crude oil, leading to frequent corrosion phenomena that have a negative impact on the equipment's ability to function normally [1,2]. As a result, corrosion-related safety incidents are increasing in frequency in the refining sector, making their resolution a pressing issue for refineries. Different types of corrosion will develop in different areas of the refinery depending on how materials interact with the environment. The impact of corrosive chemicals on matrix materials has been a topic of discussion among academics for a while [3]. Carbon steel is more affordable than other types of steel, and it is now the most often used metal for pipelines and refinery equipment [4,5]. Low carbon steel has a weak corrosion resistance, which is unfortunate [6,7]. Low carbon steel often corrodes more quickly in the presence of NH_4Cl.

NH_3 and HCl components in the gas phase will crystallize to create NH_4Cl particles, which will then deposit on the inner surface of the pipeline or other machinery [8-11]. Strongly hygroscopic and easily absorbed by water, the deposited NH_4Cl quickly creates a highly concentrated corrosive solution that eats away at the device's oxide film and causes electrochemical corrosion [12,13]. The corrosion failure issue brought on by NH_4Cl deposition is severe, and it is thought to be a significant factor in the corrosion failure of pipelines and equipment made of low carbon steel [14]. It also has a detrimental impact on the functionality of refinery equipment [15]. For many years, NH_4Cl-induced corrosion has harmed the machinery and pipelines of several refining units, including crude oil distillation units, hydrogenation treatment systems [1], and catalytic cracking units [16]. This has led to a number of unintended risks and losses. As a result, in-depth study on ammonium chloride corrosion must be done, and suitable steps must be taken to lessen the effect of NH_4Cl on the apparatus [17].

Many academics have been researching the NH_4Cl corrosion of low carbon steel refining units at the moment. In addition to discovering NH_4Cl-related corrosion in the distillation column, Kimmel et al. [18] also discovered NH_4Cl-related corrosion in ammonia synthesis equipment operating at high temperatures and high pressures. After researching the corrosion failure of the hydrogenated high-pressure air cooler system, Liu et al. [19] discovered that ammonium chloride deposition was the root cause of the corrosion failure. The corrosion failure of ammonium chloride in the hydrocracking unit was investigated

[1] CHANGZHOU UNIVERSITY, SCHOOL OF ENVIRONMENTAL SCIENCE AND ENGINEERING, CHANGZHOU, 213164, CHINA
[2] CHANGZHOU UNIVERSITY, SCHOOL OF MECHANICAL ENGINEERING AND RAIL TRANSIT, CHANGZHOU, 213164, CHINA
* Corresponding author: jstgyx123@163.com

by Zhu et al. [1]. Many academics have used simulation tools like Aspen and CFD to research the temperature at which ammonium chloride crystallizes and the location at which its depositions in order to analyze the corrosion of ammonium chloride.

It is referred to as "acidic water" when effluent from the refinery that contains ammonia, carbon dioxide, and hydrogen chloride is created. Each component of the refinery will generate a sizable amount of acidic water during the refining process. In order to post-treat the sewage and lower the concentration of contaminants, the sewage stripping procedure is necessary [20]. The sour water stripper has developed into one of the crucial pieces of equipment for eliminating HCl, NH_3, CO_2, and other corrosive gases in the refinery as it serves as the main component of the sewage stripping process [21]. Where these contaminants come into touch with the substrate material of the stripper, such as top trays, pipes, and other components, corrosion invariably takes place. Low carbon steel is typically used as the matrix material for the machinery and pipelines of the top system of the sour water stripper.

The majority of relevant research, however, focuses on hydrocracking units and columns for the distillation of crude oil; ammonium chloride corrosion of low-carbon steel pipes in acid water stripping units is rarely studied. The high corrosion rate continues to be a major threat to the stripping unit's normal operation and process safety, and the NH_4Cl corrosion problem has not been satisfactorily resolved in the acidic water stripping unit. Currently, China lacks a systematic study on the micro-corrosion process and affecting factors of NH_4Cl corrosion under stripping conditions. There is still a dearth of comprehensive knowledge and pertinent experimental data about the corrosion process that these parameters affect.

The corrosion behavior of 20# carbon steel, the sour water stripper's matrix material, in NH_4Cl solution at various temperatures and concentrations was examined in this study. A variety of analytical techniques were used to characterize the corrosion site's morphology and corrosion products. Tafel polarization method and electrochemical impedance spectroscopy (EIS) were employed to study the electrochemical corrosion characteristics of 20# carbon steel. The goal of this work is to investigate the ideal operating conditions for the sour water stripper in the NH_4Cl environment and to provide valuable corrosion experimental data for the study of ammonium chloride corrosion in the stripper pipeline through the simulation experiment of corrosion reaction in the real NH_4Cl environment.

2. Materials and methods

2.1. Experimental preparation and measuring instruments

The chemical composition of the metal material at the top of the stripper was examined in accordance with GB/T 40802-2021 to ascertain its dependability. The sample with a size of 12 mm × 12 mm × 12 mm was intercepted at the corrosion site of the sour water stripper. Grinding and polishing step by step with water sandpaper to remove burrs. After that, the sample was degreased in an organic solvent, and a certain concentration of acid solution was used to immerse the sample to remove the corrosion products. After washing, dehydration and hot air drying, it is stored in the dryer for use. Scanning electron microscope (SEM) and X-ray energy dispersive spectrometer (EDS) observations of the surface topography and elemental composition of corroded specimens. The sample's component composition was examined using an X-ray diffractometer (XRD) model D/max2500.

2.2. Electrochemical measurements

Sour water stripper corrodes mostly due to electrochemical damage brought on by a change in the metal's chemical environment. Determining the environment in which the corrosion occurs is therefore required before the electrochemical test. Since the principal corrosive medium is NH_4Cl, temperature and solution concentration are two crucial factors impacting the corrosive environment. Therefore, in order to imitate the actual production environment for the corrosion of the top of the sour water stripper, a specific temperature and concentration of NH_4Cl solution are used in this paper. Tafel polarization and EIS were used to examine the electrochemical corrosion characteristics of the matrix material, 20# carbon steel. The NH_4Cl solution's concentration and temperature were the variables put to the test.

The DH7000C electrochemical workstation and a three-electrode system were used to conduct the electrochemical testing. Saturated calomel electrode (SCE) served as the reference electrode, while platinum electrode served as the auxiliary electrode and 20# carbon steel served as the working electrode, with an exposed surface of roughly 0.2826 cm^2. Fig. 1 depicts a schematic of a three-electrode system. The chemical breakdown of 20# steel is displayed in TABLE 1, and its density is 7.85 g/cm^3.

Tafel polarization was measured after open circuit voltage had stabilized. The scanning rate was 0.333 mV/s, and the

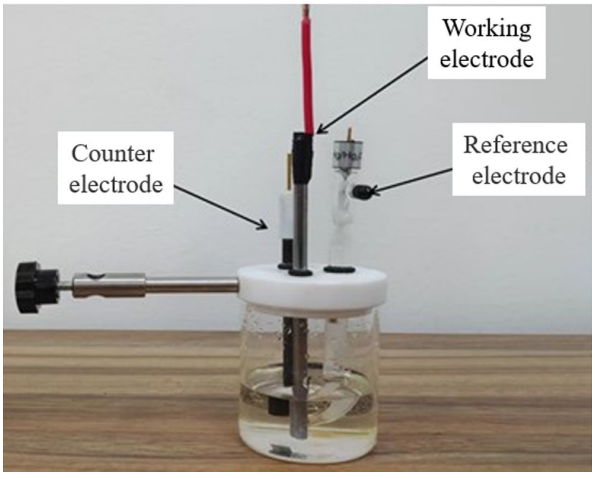

Fig. 1. The sketch of three-electrode system

TABLE 1

Chemical composition (wt.%) of working electrode

Composition	Ni	Cr	Cu	S	P	C	Mn	Si
Content	≤0.30	≤0.25	≤0.25	≤0.03	≤0.035	0.17-0.23	0.35-0.65	0.17-0.37

TABLE 2

Chemical composition (wt.%) of 20 # carbon steel before and after corrosion

Composition	S	P	Cr	Ni	Cu	C	Mn	Si
Before	≤0.03	≤0.035	≤0.25	≤0.30	≤0.25	0.17-0.23	0.35-0.65	0.17-0.37
After	0.03	0.025	0.18	0.22	/	0.18	0.55	0.29

potential ranged from –0.25 to 0.25 V. After tests, the Tafel extrapolation method was used to determine the corrosion rate. EIS was lastly polled. The fluctuation was 5 mV, and the periodicity varied from 10^5 to 10^{-2} Hz.

3. Results and discussions

3.1. Chemical composition of material

In TABLE 2, the elemental makeup of 20# carbon steel at the corrosion site is displayed. The findings demonstrate that the material's constituents fall within the acceptable content range. As a result, the sour water stripper does not have a manufacturing flaw, and the corrosive medium is to blame for the device's degradation.

3.2. Surface topography and element components

Fig. 2 displays the surface topography and element distribution of the scale in the sour water stripper. SEM picture of the sample is presented in Fig. 2(a). On the surface of 20# carbon steel, there are several pitting pits of all sizes, and even two pitting pits have grown larger, with the larger ones forming roughly 14 μm voids, as can be seen from the SEM topography. The non-uniform portion of the corrosion region is represented by spectrum area 1. It demonstrates that the 20# carbon steel's surface has rusted. The sample's EDS spectrum appears in Fig. 2(b). The findings indicate that the scale contains the elements O, C, Ni, Fe, Cr, Cl and Al, with O being the most abundant. This demonstrates that the oxidation reaction occurs when the corrosion areas of the gadget are exposed to air during maintenance.

3.3. Compound composition

Scaling is present on the corrosion pipeline at the top of the sour water stripper, and the scale is black-brown in color. In Fig. 3, the XRD pattern is displayed. The outcome demonstrates that the sample's primary components are Fe_3O_4, $FeCl_2$, NH_4Cl and Fe_2O_3. The fact that the Fe_3O_4 is black and matches the color of the pipe scale proves that the diffraction peak is calibrated properly. The reaction between a metal wall and HCl gas in a humid environment produces $FeCl_2$. HCl and NH_3 in gas crystallize, producing NH_4Cl as a result. During maintenance, the oxidation process of the pipeline with air produces iron oxides. The compound's composition agrees with the element distribution from earlier.

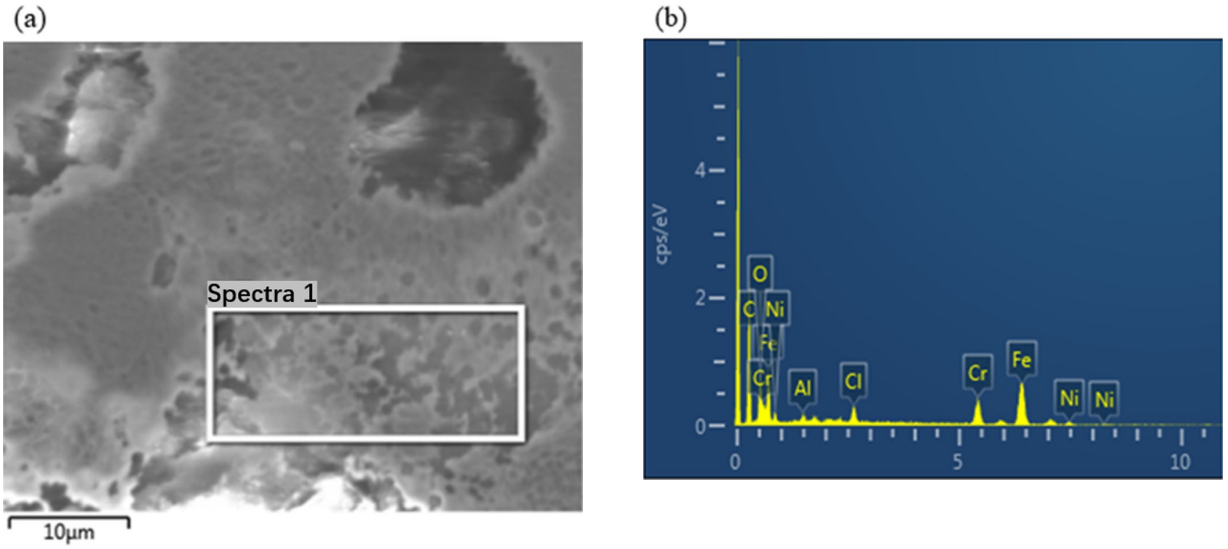

Fig. 2. (a) SEM morphologies of steel, (b) EDS spectrum of elemental composition

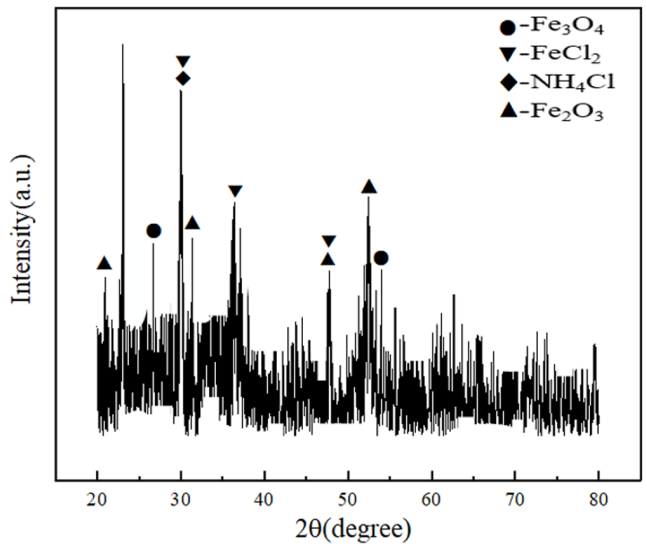

Fig. 3. XRD pattern of corrosion products of sour water stripper pipeline

3.4. Tafel polarization curves

3.4.1. Impact of temperature

In order to study the electrochemical decline law of 20# steel at various temperatures, the solution concentration was held to 5%. The Tafel polarization curve of 20# steel at various temperatures is depicted in Fig. 4(a). Etch rates were computed using data from the Tafel polarization curve. As illustrated in Fig. 4(b), the curves of corrosive current density (I_{corr}), potential (E_{corr}) and rate with temperature is obtained.

As can be seen from Fig. 4(a), the 20# steel Tafel polarization curve is identical between 20°C and 80°C. The electrochemical corrosion of 20# steel involves oxygen depolarization corrosion. The cathode process is regulated by oxygen diffusion, while the anode process is governed by the active dissolution of metal. In other words, cathode concentration polarization governs the rate of corrosion. The corrosion rate increases by 4.1885 mm/a and I_{corr} increases by 360.63 A/cm^2 when the temperature rises to 80°C from 20°C, according to the findings of Fig. 4(b). E_{corr} also falls by 3.11 mV. This is because ammonium chloride is a strong electrolyte, its aqueous solution is weakly acidic. Increasing the temperature will shift the ionization equilibrium of the solution and produce a large amount of hydrogen ions, which will react with the active metals in 20# carbon steel. The protective coating on the metal surface gradually dissolves as the temperature rises. When the oxide coating loses its barrier function, the metal electrode reaction and oxygen diffusion process speed up. As a result, material erosion rate improves.

3.4.2. Impact of NH_4Cl density

By regulating the temperature to the actual temperature of the device at 40°C, the electrochemical corrosion actions of 20# steel in various densities were examined. The Tafel polarization curve of 20# steel at various densities appears in Fig. 5(a). The corrosion rate was calculated using the Tafel polarization curve data. It can produce the curves of I_{corr}, E_{corr} and corrosion rate with density, as illustrated in Fig. 5(b).

The Tafel polarization curves of various densities are essentially the same, as seen in Fig. 5(a). It suggests that varying densities of 20# steel have a comparable corrosion mechanism. I_{corr} increases by 459.33 μA/cm^2, E_{corr} lowers by 2.92 mV, and the corrosion rate rises by 5.6052 mm/a as the concentration rises from 5% to 20%, as seen in Fig. 5(b). The oxidation reaction of the anode metal Fe and the reduction reaction of the cathode H^+ are recognized to be the electrochemical corrosion reactions in the three-electrode system. The concentration of hydrogen ions grows together with the NH_4Cl concentration, which raises the potential of the hydrogen electrode. The depolarization reaction of the cathode in the solution is accelerated when the hydrogen overpotential is constant due to an increase in driving force. As a result, corrosion occurs faster.

The solution is acidic because NH_4Cl is a strong acid and a weak alkali salt. The acidity and corrosivity increase in direct proportion to the amount of NH_4Cl present. The concentration of Cl^- rose along with the concentration of NH_4Cl as enrichment and adsorption took place on the surface of 20# carbon steel. This

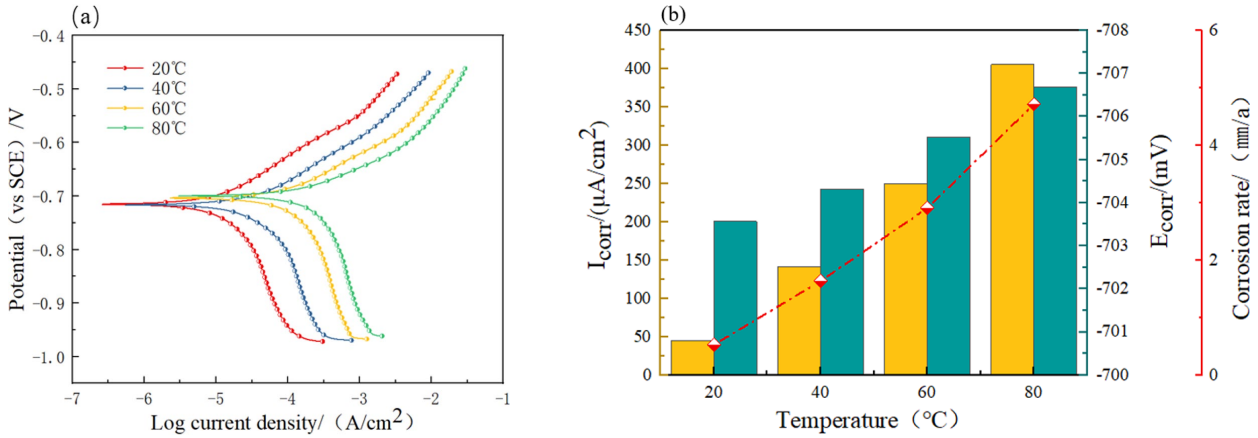

Fig. 4. Curves of 20# steel at 20, 40, 60 and 80°C in 5% NH_4Cl solution. (a) Tafel polarization, (b) Corrosion current density (I_{corr}), potential (E_{corr}) and rate

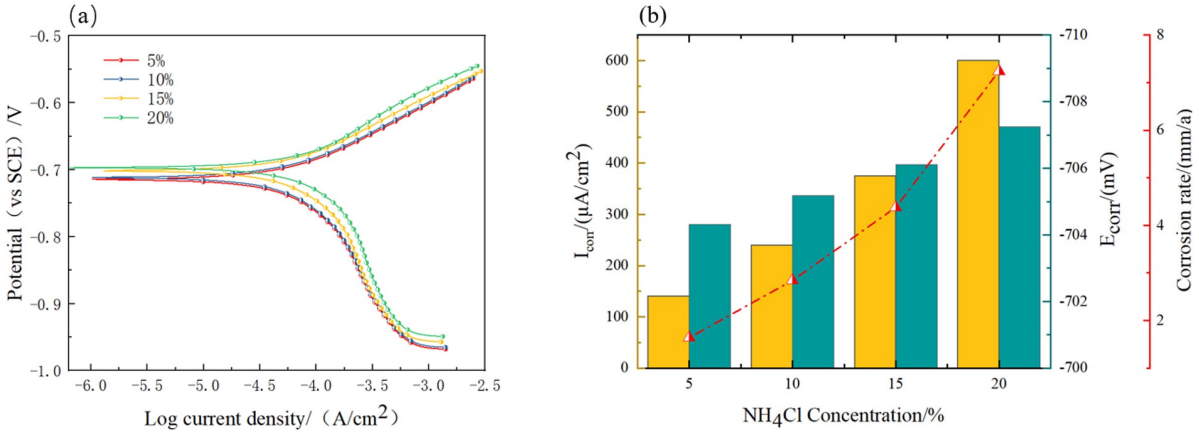

Fig. 5. Curves of 20# steel at 40°C in solutions of 5, 10, 15 and 20% NH_4Cl (a) Tafel polarization, (b) Corrosion current density (I_{corr}), potential (E_{corr}) and rate

led to the breakdown of the passivation film on the surface and a reduction in the passivation film's ability to protect the surface. Additionally, as the pH falls, it furthers local acidity, creating a blocking action that makes it simple to dissolve locally and produce numerous pitting pits.

3.5. Electrochemical impedance spectroscopy

3.5.1. Effect of temperature

Impedance spectrum is typically an imperfect semi-circular arc. The sample's resistance to corrosion improves with increasing diameter. To investigate the electrochemical behavior of the material contact, an EIS test was run on 20# steel. The Nyquist curve and related parameter change diagram of 20# steel at various temperatures and 5% solution concentrations are displayed in Fig. 6.

In Fig. 6(a), there are two semi-circular arcs with various amplitudes for each Nyquist curve. The radius of the first capacitance arc steadily reduces as temperature rises to 80°C from 20°C, and the radius of the second semicircle becomes more pronounced. This suggests a change in the interfacial mechanism between the pole and the electrolyte. This is due to the charge transfer mechanism being crucial at low temperatures, where the concentration polarization effect may be disregarded. The concentration polarization effect is increasingly prominent as the temperature rises. As the temperature grows, Fig. 6(b) shows that the solution internal resistance (R_s) between the reference and working electrodes drops, the charge transfer impedance (R_{ct}) lowers as well, and the double layer capacitance (C_d) steadily rises. The diffusion coefficient and the activity of the reactive ions in the solution will both increase as the temperature rises. speeding ion migration, encouraging ions to flow through the electric field, and degrading the working electrode's surface as a result. As the temperature rises, the working electrode's anti-corrosion property steadily deteriorates and the rate of corrosion accelerates. The test outcomes are in agreement with the Tafel polarization under the previously mentioned circumstances.

3.5.2. Effect of NH_4Cl concentration

Studying the AC impedance spectra and related parameters of 20# steel in various concentrations was done at a temperature controlled to 40°C. The results appear in Fig. 7. Each Nyquist

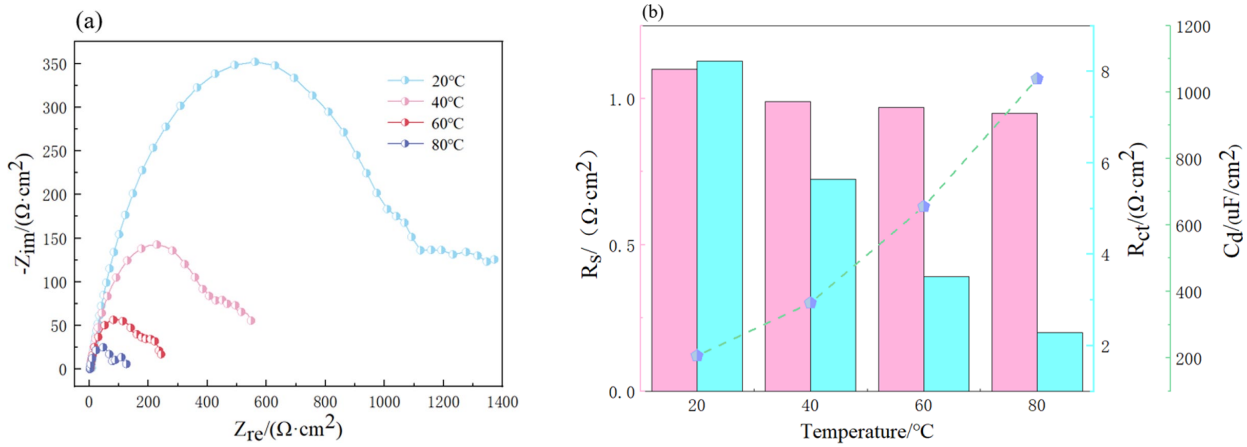

Fig. 6. Curves of 20# steel at 20, 40, 60 and 80°C in 5% NH_4Cl solution. (a) AC impedance spectra, (b) Solution internal resistance (R_s), charge transfer impedance (R_{ct}) and double layer capacity (C_d)

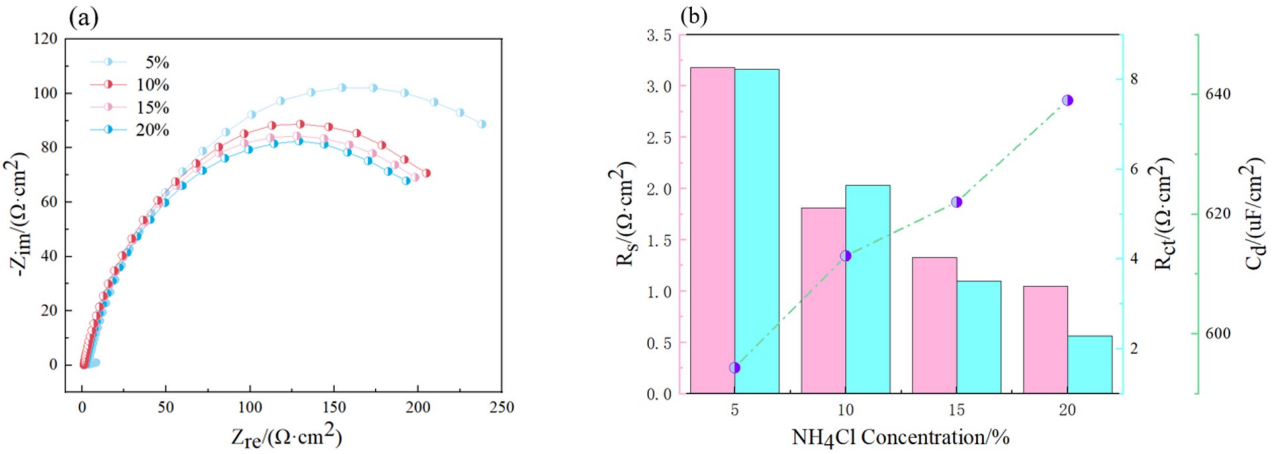

Fig. 7. Curves of 20# steel in 5, 10, 15 and 20% NH_4Cl solutions at 40°C. (a) AC impedance spectra, (b) Solution internal resistance (R_s), charge transfer impedance (R_{ct}) and double layer capacity (C_d)

curve in Fig. 7(a) depicts a clear capacitive reactance arc, and as the solution concentration rises from 5% to 20%, the radius of the arc gradually gets smaller. As concentration rises, R_s and R_{ct} constantly drop, as can be observed in Fig. 7(b). This demonstrates how the rate of corrosion of 20# steel is sped up. The converse is true for the change law of C_d, which has a positive correlation with concentration. This is due to the fact that metal corrosion gets worse as Cl^- concentration rises. The presence of Cl^- will prevent the formation of protective film and weaken the force between metal and corrosion products. The electrode/solution boundary layer thins as a result of the destruction of the passivation film of 20# steel and its film created with water, increasing the metal electrode's interface capacitance. Therefore, the metal's electrochemical reaction is made easier by a higher solution density. The working electrode's surface response process is accelerated, which speeds up the material's rate of corrosion.

4. Conclusions

This study used electrochemical methods to analyze the erosion behavior of 20 # carbon steel in NH_4Cl solution using chemical composition analysis, EDS, SEM, and XRD detection technology. The findings allow for the following inferences:

(1) According to the SEM findings, the acid water stripping device causes corrosion and surface destruction to the matrix material's 20# carbon steel during use. On the metal's surface, there are local perforations as well as pitting pits.

(2) According to EDS and XRD data, the corrosion site contains O, C, Ni, Fe, Cr, Cl, and Al, with O having a greater concentration. $FeCl_2$ was the device's corrosion byproduct, and the oxidation reaction occurred while it was being maintained.

(3) Tafel polarization and EIS data demonstrate that temperature and solution concentration have the greatest impact on the corrosion rate of 20# carbon steel in an ammonium chloride environment. To prevent salt deposition and lessen the corrosion of ammonium chloride at the top of the sour water stripper, the temperature and solution concentration at the device's operation site can be maintained at a low level.

(4) The system's reactive ions were more active, the passivation film was more active and easier to erode, and the corrosion rate increased by 4.1885 mm/a when the temperature of the ammonium chloride solution rose from 20°C to 80°C.

(5) The amount of Cl^- in the solution increased as the ammonium chloride concentration in the solution rose from 5% to 20%. Chloride ions were enriched and adsorbed on the surface of 20# carbon steel, resulting in the breakdown of the passivation film on the metal surface, and the corrosion rate of 20# carbon steel increased by 5.6052 mm/a. As far as the research scope of this paper is concerned, the concentration of ammonium chloride has a greater influence on the corrosion rate of 20# carbon steel than the solution temperature.

Acknowledgment

This work was supported by the National Natural Science Foundation of China (Grant No. U1909216).

REFERENCES

[1] M. Zhu, G.F. Ou, H.Z. Jin, K.X. Wang, Z.J. Zheng, Eng. Fail. Anal. **57**, 483-489 (2015).
DOI: https://doi.org/10.1016/j.engfailanal.2015.08.022

[2] H.Z. Jin, X.P. Chen, J. Ren, X.H. Wu, Z.J. Zheng, G.F. Ou, Y.S. Ye, Braz. J. Chem. Eng. **35** (3), 1051-1062 (2018).
DOI: https://doi.org/10.1590/0104-6632.20180353s20160661

[3] R.D. Li, H. Huang, X.D. Wang, Y.S. Wang, Corros. Sci. **203**, 110362 (2022).
DOI: https://doi.org/10.1016/j.corsci.2022.110362

[4] X.Q. Xu, Z.Q. Bai, Y.R. Feng, Q.R. Ma, W.Z. Zhao, Appl. Surf. Sci. **280**, 641-645 (2013).
DOI: https://doi.org/10.1016/j.apsusc.2013.05.038

[5] W. Geary, Eng. Fail. Anal. **1**, 249-256 (2013).
DOI: https://doi.org/10.1016/j.csefa.2013.09.001

[6] Y. Zhao, W. Qi, J. Xie, Y. Chen, T. Zhang, D. Xu, F. Wang, Corros. Sci. **166**, 108448 (2020).
DOI: https://doi.org/10.1016/j.corsci.2020.108448

[7] A.H. Alamri, Eng. Fail. Anal. **116**, 104735 (2020).
DOI: https://doi.org/10.1016/j.engfailanal.2020.104735

[8] A.A. Ahmed, ARO-Sci. J. Koya. Univ. **9**, 21-27 (2021).
DOI: https://doi.org/10.14500/aro.10711

[9] S. Addepalli, D. Eiroa, S. Lieotrakool, A.L. Francois, J. Guisset, D. Sanjaime, M. Kazarian, J. Duda, R. Roy, P. Phillips, Proc. CIRP. **38**, 137-142 (2015).
DOI: https://doi.org/10.1016/j.procir.2015.07.057

[10] M. Javidi, M.A. Sadeghi, R. Jafari, A.A. Hoodi, Eng. Fail. Anal. **115**, 104678 (2020).
DOI: https://doi.org/10.1016/j.engfailanal.2020.104678

[11] Z.J. Zheng, G.F. Ou, H.J. Ye, J.L. Tan, H.Z. Jin, Eng. Fail. Anal. **79**, 726-736 (2017).
DOI: https://doi.org/10.1016/j.engfailanal.2017.05.018

[12] K. Toba, M. Ueyama, K. Kawano, J. Sakai, Corrosion. **68** (11), 1049-1056 (2012). DOI: https://doi.org/10.5006/0587

[13] H.Z. Jin, X.P. Chen, G.F. Ou, J.Q. Zhang, Eng. Fail. Anal. **109**, 104274 (2020).
DOI: https://doi.org/10.1016/j.engfailanal.2019.104274

[14] S.A. Treese, Petrol. Technol. Quarterly **3**, 57-65 (2019).

[15] H.Y. Zhu, H.Z. Jin, S.X. Zhang, X.F. Liu, C. Wang, Chem. Eng. Sci. **269**, 118455 (2023).
DOI: https://doi.org/10.1016/j.ces.2023.118455

[16] G.F. Ou, K.X. Wang, J.L. Zhan, M. Tang, H.H. Liu, H.Z. Jin, Eng. Fail. Anal. **31**, 387-393 (2013).
DOI: https://doi.org/10.1016/j.engfailanal.2013.02.025

[17] A.H. Al-Moubaraki, I.B. Obot, J. Saudi. Chem. Soc. **25** (12), 101370 (2021).
DOI: https://doi.org/10.1016/j.jscs.2021.101370

[18] A.-C.L. Kimmel, T.F. Malkowski, S. Griffiths, B. Hertweck, T.G. Steigerwald, L.P. Freund, S. Neumeier, M. Goken, J.S. Speck, E. Schluecker, J. Cryst. Growth. **498**, 289-300 (2018).
DOI: https://doi.org/10.1016/j.jcrysgro.2018.06.018

[19] X.F. Liu, K. Luo, J.R. Fan, Int. J. Multiphas. Flow. **87**, 250-262 (2016).
DOI: https://doi.org/10.1016/j.ijmultiphaseflow.2016.09.012

[20] M. Zhu, L. Sun, G.F. Ou, K. Wang, K.X. Wang, Y.L. Sun, Eng. Fail. Anal. **62**, 93-102 (2016).
DOI: https://doi.org/10.1016/j.engfailanal.2016.01.002.

[21] M.H. Hafiz, R.A. Majed, R.S. Noor, M.A. Wehib, Int. J. Electrochem. Sc. **8**, 12402-12416 (2013).
DOI: https://doi.org/10.1016/S1452-3981(23)13276-7